

The modification of structural and optical properties of nano- and submicron ZnO powders by variation of solvothermal syntheses conditions

D. Luković Golić · J. Ćirković · M. Šćepanović ·
T. Srećković · E. Longo · J. A. Varela · N. Daneu ·
V. Stamenković · G. Branković · Z. Branković

Received: 25 April 2014 / Accepted: 20 September 2014 / Published online: 1 October 2014
© Springer Science+Business Media Dordrecht 2014

Abstract Nano- (30–60 nm) and submicron (100–350 nm) ZnO particles were synthesized using solvothermal method at 200 °C from an ethanolic solution of zinc acetate dihydrate, applying different reaction conditions, i.e., pH value of precursor and time of the reaction. The X-ray diffraction (XRD), field emission scanning electron microscopy (FE-SEM), transmission electron microscopy (TEM), UV–vis diffuse reflectance (DR), Raman spectroscopy, and photoluminescence (PL) spectroscopy have been employed for characterization of

synthesized ZnO powders. It was shown that the structural, morphological, and optical properties are largely determined by reaction conditions during solvothermal synthesis. The particle crystallinity improves with the decrease of pH value and/or the increase of time of the reaction. The Raman and PL spectra analyses indicate that the oxygen interstitials are dominant intrinsic defects in solvothermally synthesized ZnO powders. It was observed that concentration of defects in wurtzite ZnO crystal lattices slightly changes with the variation of pH value of the precursor and time of the solvothermal reaction. The correlation between structural ordering and defect structure of particles and corresponding growth processes was discussed.

D. Luković Golić (✉) · J. Ćirković · T. Srećković ·
G. Branković · Z. Branković
Institute for Multidisciplinary Research, University of
Belgrade, Kneza Višeslava 1a, 11030 Belgrade, Serbia
e-mail: danijeluk@gmail.com

M. Šćepanović
Center for Solid State Physics and New Materials,
Institute of Physics, University of Belgrade, Pregrevica
118, 11080 Belgrade, Serbia

E. Longo · J. A. Varela
Departamento de Físico-Química-IQ, Universidade
Estadual Paulista, P. O. Box 355, Araraquara,
SP 14801-907, Brazil

N. Daneu
Jožef Štefan Institute, Jamova 39, 1000 Ljubljana,
Slovenia

V. Stamenković
Materials Science Division, Argonne National
Laboratory, Argonne, IL 60439, USA

Keywords ZnO · Nano- and submicron particles ·
Solvothermal synthesis · Growth mechanism ·
Structure ordering · Photoluminescence

Introduction

Zinc oxide (ZnO) is a wide band gap ($E_g = 3.37$ eV at room temperature, near-UV spectral region) semiconductor with high exciton binding energy (60 meV) enabling persistence of excitonic emission processes at or above room temperature (Mang et al. 1995). It has great potential for various applications, such as UV-light emitters, photocatalysts, surface acoustic wave

devices, piezoelectric transducers, optical waveguides (Nickel and Terukov 2005; Jagadish and Pearton 2006), etc. Various properties and prospects for application of ZnO powders depend on crystal structure, morphology, and defect structure of ZnO particles. Optical and electronic properties largely depend on types and concentration of defects in ZnO crystal lattice. Consequently, the defect structure of the lattice must be controlled, and that includes optimization of the synthesis conditions. The processes taking place during particle growth are responsible for structural and morphological properties of the ZnO powders, but also have an influence on defect structure.

ZnO usually exhibits UV emission commonly considered as the near-band-edge emission or the exciton recombination emission and visible emission bands attributed to the intrinsic or extrinsic defects in ZnO (Cai et al. 2012). The oxygen vacancies (V_O), zinc vacancies (V_{Zn}), interstitial oxygen (O_i), and interstitial zinc (Zn_i) were intrinsic defects responsible for visible emissions at different wavelengths in ZnO. Despite many years of investigations, the explanations for visible photoluminescence emissions are still controversial because the behavior of the defects has not been completely understood (Djurišić and Leung 2006).

In our previous investigations (Luković Golić et al. 2011; Luković Golić et al. 2012), we have shown that the morphology of nano- and submicron ZnO powders could be controlled by adjusting the solvothermal reaction conditions because these conditions define the growth mechanisms, responsible for the properties of the ZnO powders. In the present article, special attention was paid to correlation between defect structure and the solvothermal reaction conditions. It was found that pH value of precursor and time of the reaction at given temperature largely affect structural, microstructural, and optical properties, as well as the type and concentration of defects.

Experimental

Sample preparation

The following chemicals were used in solvothermal syntheses: zinc acetate dihydrate $Zn(CH_3COO)_2 \cdot 2H_2O$ (Sigma Aldrich, 99.99 %), absolute ethanol (Sigma Aldrich, ≥ 99.5 %), lithium hydroxide monohydrate, $LiOH \cdot H_2O$ (Sigma Aldrich, 99.95 %).

Table 1 The labels of ZnO powders obtained in solvothermal syntheses at 200 °C under the defined conditions (time of the reaction and pH value of the precursor)

Time of the reaction (h)	pH value	Assignment
2	12	P-2h-12
2	10	P-2h-10
2	8	P-2h-8
4	8	P-4h-8
10	8	P-10h-8
24	8	P-24h-8

The precursor for the solvothermal treatment was prepared using the modified Spanhel method (Spanhel and Anderson 1991). Solution of zinc acetate in absolute ethanol (0.1 mol dm^{-3}) was refluxed at 80 °C for 3 h under magnetic stirring. After natural cooling, the pH value was adjusted using 0.8 mol dm^{-3} LiOH solution in deionised water. Prepared solution with defined pH value was placed in a Teflon-lined, stainless-steel autoclave reactor from Roth Karlsruhe ($T_{\text{max}} = 300 \text{ °C}$, $P_{\text{max}} = 300$ bars) where control of temperature and pressure is possible. The solvothermal syntheses were realized at 200 °C during the different reaction times (2, 4, 10, and 24 h) and pH values of the precursor (8, 10, and 12). The products of solvothermal treatments were washed with deionised water and centrifuged (3,500 rpm, $t = 10$ min). White powder was obtained after drying at temperature of 80 °C.

Solvothermally synthesized ZnO powders are assigned as shown in Table 1.

Sample characterization

The powders were analyzed using XRD, FESEM, TEM, UV-vis DR, Raman spectroscopy, and PL spectroscopy. XRD patterns were recorded by Rigaku® RINT 2000 diffractometer using Ni-filtered $Cu K\alpha$ radiation ($\lambda = 1.54178 \text{ Å}$). The lattice parameters were calculated from the XRD data using the least-squares method by the LSUCRI software (Garvey 1986). Morphology was examined by a FESEM using JEOL JSM-7500F and TEM using JEM-2100 JEOL microscope. The UV-vis DR spectra were recorded in the wavelength range of 200–1,400 nm on the Shimadzu UV-2600 spectrophotometer equipped with an integrated sphere. The reflectance spectra were

measured relative to a reference sample of BaSO₄. PL measurements were performed at room temperature using Kr laser ($\lambda = 350$ nm) as the excitation source. Raman scattering measurements were performed using Jobin–Yvon T64000 triple spectrometer, equipped with a confocal microscope and a nitrogen-cooled CCD detector. The average crystallite size is estimated as the arithmetic average of the crystallite size values obtained using Scherrer equation for the strongest diffraction peaks of wurtzite ZnO, labeled as (100), (002), and (101).

Results

XRD

The XRD patterns of solvothermally synthesized ZnO powders are presented in Fig. 1. The positions of diffraction peaks in all powders coincide with the ZnO wurtzite structure (JCPDS card No. 89-1397). The intensities of XRD peaks of powders obtained from highly basic precursors (P-2h-10 and P-2h-12) are slightly smaller than the intensities of XRD peaks of powders obtained from slightly basic precursors with pH = 8.

The values of the lattice parameters (Table 2) suggest that the structural changes in investigated ZnO powders are very small. Deviations of lattice volume (ΔV) from the value reported in JCPDS card No.

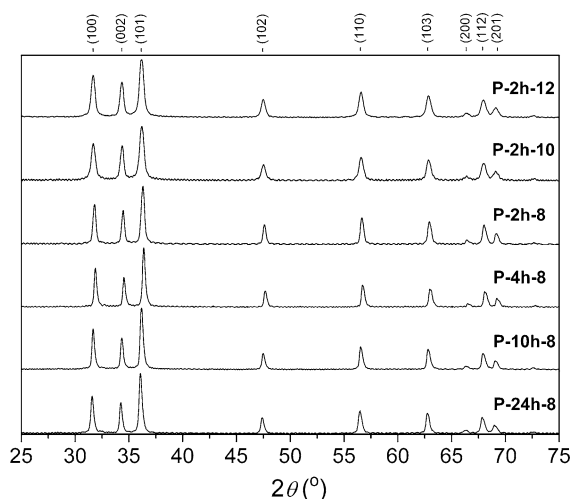


Fig. 1 XRD patterns of the ZnO powders (Table 1) synthesized by solvothermal reactions

89-1397 did not exceed 0.65 %. It means that defect structure is not expressed largely i.e., the occurrence of the intrinsic defects leads to the small modifications in the crystal lattice structure.

The full width at half maximum (FWHM) of the diffraction peaks slightly changes depending on time of the reaction, but this change is more pronounced with the variation of the precursors' pH value. Furthermore, the average crystallite size can be estimated, using the Scherrer equation, to be about 20 nm for the ZnO powders synthesized from highly basic precursors and about 30 nm for ZnO powders obtained from slightly basic precursors (Table 2).

FESEM and TEM analyzes

The FESEM images of ZnO powders characterized by different pH values are presented in Fig. 2. The powder P-2h-8 mostly consists of hexagonal, prismatic particles with diameters of 70–200 nm and lengths of 100–200 nm. The powders P-2h-10 and P-2h-12 contain rounded nanoparticles (size range, 30–60 nm), partly agglomerated. The ZnO particles from these powders are more homogenous in size and shape than particles from powder P-2h-8.

The TEM images of ZnO powders with pH = 8, in which the time of the reaction was varied, are shown in Fig. 3. The powder P-2h-8 contains prismatic particles, ranging in the above-mentioned size (Fig. 3a). The TEM image of powder P-4h-8 shows that it consists of hexagonal, prismatic particles (the diameter ranges between 150 and 350 nm) arranged in the same plane, but some of them show internal microstructure i.e., the small particles within the larger ones. Figure 3c indicates coexistence of hexagonal, prismatic particles (the larger ones with diameter of about 250 nm and smaller ones with diameter between 50 and 100 nm) and small number of rod-like particles (length less than 100 nm) in the powder P-10h-8. Extension of time reaction to 24 h led to the formation a large number of the rod-like particles (Fig. 3d) (length ranges between 200 and 350 nm, diameters less than 100 nm). HRTEM images of ZnO powders P-4h-8, P-10h-8, and P-24h-8 (Fig. 4) point out the shape and size of the dominant type of particles for each powder. These results are in accordance with the previous statements derived from TEM images.

Correlation between microstructure of the ZnO powders and reaction conditions was already

Table 2 The parameters of wurtzite crystal lattices for solvothermally synthesized ZnO powders (calculated using the LSUCRI program) and average crystallite size (estimated by Scherrer equation)

ZnO powders	a (Å)	c (Å)	V (Å ³)	ΔV (%)	Crystallite size (nm)
Card no. 89-1397	3.253	5.213	47.77	–	–
P-2h-12	3.253 (1)	5.208 (3)	47.73 (4)	–0.08	19
P-2h-10	3.252 (1)	5.207 (3)	47.70 (4)	–0.15	19
P-2h-8	3.2496 (5)	5.205 (1)	47.60 (1)	–0.36	27
P-4h-8	3.2469 (9)	5.198 (2)	47.46 (3)	–0.65	31
P-10h-8	3.255 (1)	5.213 (2)	47.84 (3)	+0.15	29
P-24h-8	3.257 (2)	5.224 (4)	48.00 (6)	+0.48	29

discussed in our previous article (Luković Golić et al. 2012) where we have concluded that pH value and reaction time affect the shape and size of the ZnO particles, considerably. Obviously, increasing of the pH value from 8 to 10 and 12 leads to the change in the shape, from regular hexagonal prisms to more rounded shapes (Fig. 2). Additionally, the particles' shape changes from hexagonal prisms (P-2h-8, P-4h-8 and P-10h-8) to rod-like forms (P-24h-8) with the extension of reaction time (Figs. 3, 4). The mean particle size (Fig. 3) of these ZnO powders increases with the extension of the reaction time.

UV–Vis DR spectroscopy analysis

The influence of the particle size and morphology on the optical properties of ZnO was examined by UV–vis DR spectroscopy. The direct band gap energies (E_g) were calculated by the Kubelka–Munk method from Tauc plot (Wood and Tauc 1972).

The UV–vis DR spectra of ZnO powders after Kubelka–Munk transformation are shown in Fig. 5 as a Tauc plot, which presents modified Kubelka–Munk function $[F(R)hv]^2$ versus photon energy, hv . The values of the direct band gap, E_g , (presented in Table 3) were obtained as the point of intersection of the tangent line on Tauc plot and the horizontal axis. Band gaps for all ZnO samples are narrower than the band gap of bulk ZnO at room temperature ($E_g = 3.37$ eV). The experimentally determined values of energy gaps for ZnO powders slightly differ from each other only on second decimal place. The energy gap obtained for the ZnO powders with higher pH values equals to 3.28 eV, and it ranges from 3.23 to 3.26 eV for the ZnO powders with pH = 8. Generally, the width of the optical band gap depends on crystallite

size, morphology, and concentration of defects in the crystal lattice (Dutta et al. 2009; Roth et al. 1982; Kumar et al. 2013). The widening of the band gap occurs due to quantum confinement effect which is expected to be predominant for very small ZnO crystallites (crystallite size less than 6 nm) (Lin et al. 2005). On the contrary, the presence of intrinsic defects in lattice results in narrowing of band gap (Šćepanović et al. 2011). Considering that all investigated ZnO powders contain relatively large crystallites (≥ 19 nm), we have supposed that the influence of defect structure on band gap width is more pronounced than the influence of quantum confinement effect.

Raman spectroscopy analysis

Raman spectra of the ZnO powders with varying pH values or time of reaction are shown in Fig. 6a, c. All observed Raman features in these spectra can be ascribed to ZnO wurtzite structure, excepting the mode at about 935 cm^{-1} which can be correlated to residual, unwashed acetate groups (Luković Golić et al. 2011).

Generally, the frequency, shape, linewidth, and relative intensity of the ZnO Raman modes can give information about disorder and defects in the crystal-line structure of this material. The frequency and linewidth of E_2^{high} mode are very sensitive to the presence of different kinds of intrinsic defects, whereas the intensity ratio of the second to the first-order LO Raman modes is indication of structural disorder of ZnO crystal structure (Šćepanović et al. 2010).

In the Raman spectra of all ZnO powders under examination, the E_2^{high} mode is positioned at about 438.2 cm^{-1} , with frequency variation within the

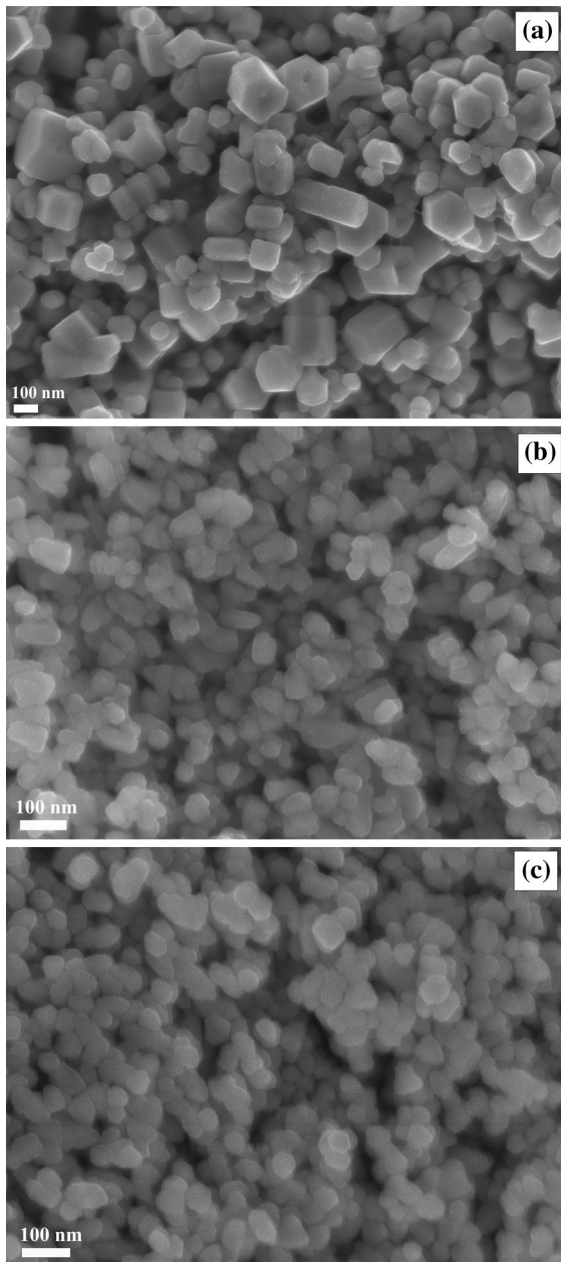


Fig. 2 FESEM images of the ZnO powders: **a** P-2h-8, **b** P-2h-10, and **c** P-2h-12

experimental error, as shown in Fig. 6b, d. This value is very close to the frequency of E_2^{high} mode in ZnO bulk crystal (438 cm^{-1} (Cusco et al. 2007)). However, linewidth of this mode in all investigated ZnO powders is greater than the mode width in ZnO bulk (6.5 cm^{-1} (Cusco et al. 2007)) and varies with pH value and time of reaction. The E_2^{high} mode broadness

from 8.3 cm^{-1} (P-2h-8), over 8.9 cm^{-1} (P-2h-10), to 9.4 cm^{-1} (P-2h-12) with the increase of pH value from 8 to 12, as shown in Fig. 6b. On the contrary, the width of E_2^{high} mode decreases from 8.3 to 7.1 cm^{-1} with the increase of the reaction time from 2 to 24 h (Fig. 6d).

The dependance of the intensity ratio of the second to the first-order LO Raman modes, $I_{2\text{LO}}/I_{1\text{LO}}$, on the pH value and synthesis duration is presented in Fig. 6b, d, respectively. These figures clearly show that $I_{2\text{LO}}/I_{1\text{LO}}$ ratio decreases with the pH value increase and increases with extension of reaction time.

PL spectroscopy analysis

The room temperature PL spectra of ZnO powders excited by 350 nm (3.54 eV) line of krypton-ion laser are shown in Fig. 7. Precisely, Fig. 7a, b displays PL spectra of ZnO powders related to the different pH values of the precursor and different times of the reaction, respectively. All recorded PL spectra are fitted on sum of two Gaussian peaks, the orange one and the green one, in all recorded PL spectra, excluding the case of powder P-24h-8 which contains additional small UV emission band. The intensities of orange and green peaks enhance with the increase of the pH value from 8 to 12, and they have maximal values in the powder P-2h-12. On the contrary, the lowest intensity of the PL peaks in visible range has been observed in the powder P-24h-8, which had the longest time of the reaction.

The energies that correspond to the maxima of the orange (E_{orange}) and green (E_{green}) PL emission, as well as the difference between those energies and the values of the energy band gap (E_g) for all investigated samples are presented in Table 3.

The position and intensity of emission peaks in PL spectra provide partial insight into the defect structure of crystal lattice of the ZnO powders. The variation of the PL intensities indicates the variation of intrinsic defects' concentration. However, many different opinions about origin of visible PL emissions were presented in literature, and various types of defects, responsible for the same colored emission, were reported. In regard to the orange emission, some authors (Djurišić et al. 2006; Greene et al. 2003; Sim et al. 2007; Shim et al. 2003) mutually agree in the opinion that orange emission appears in oxygen-rich ZnO samples. The excess oxygen in ZnO samples usually places in interstitial position of crystal lattice

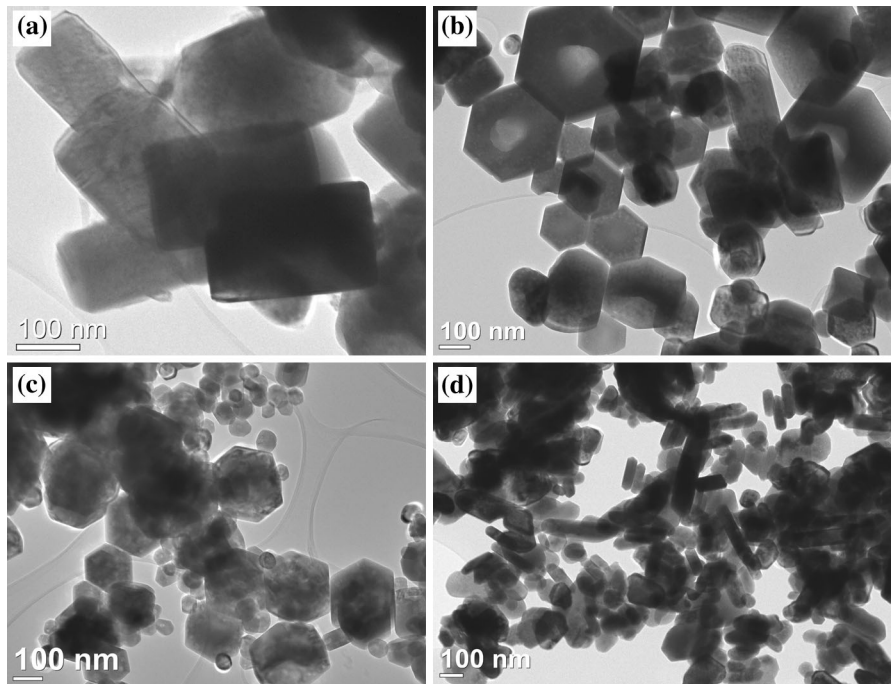


Fig. 3 TEM images of the ZnO powders: **a** P-2h-8, **b** P-4h-8, **c** P-10h-8, and **d** P-24h-8

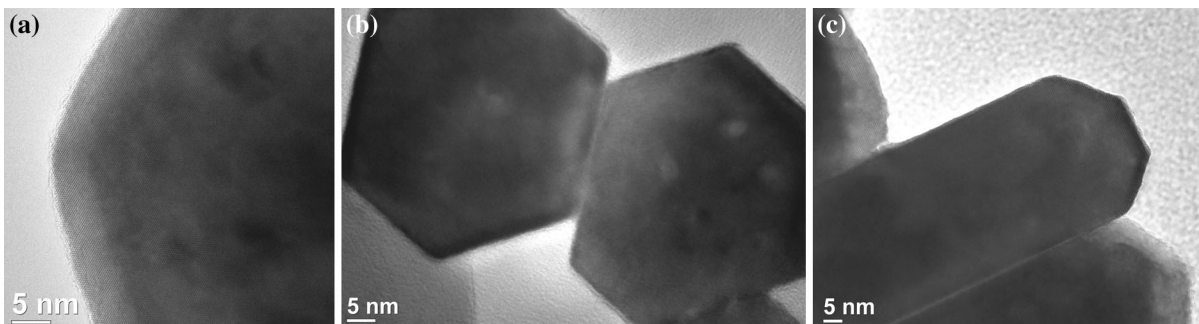


Fig. 4 HRTEM images of the ZnO powders: **a** P-4h-8, **b** P-10h-8, and **c** P-24h-8

(Studenikin et al. 1998; Panigrahy et al. 2010). Oxygen interstitials (O_i) exist either as electrically inactive, O_i^0 , in *P*-type ZnO materials or as deep acceptors at octahedral interstitial site, O_i^{2-} (oct), in *N*-type ZnO materials (Janotti and Van de Walle 2007). The energies of the orange emission for all solvothermally synthesized ZnO powders are ranging from 2.02 to 2.07 eV (see Table 3).

On the other side, the energies of the green emission of synthesized ZnO powders are ranging from 2.34 to 2.46 eV (see Table 3). The origin of the green PL emission, as the most commonly observed defect

emission in ZnO nanostructures, is quite controversial. In the recent studies (Ghosh et al. 2013; Motaung et al. 2014; Panigrahy et al. 2010), this emission is associated with singly ionized oxygen vacancies V_O^+ and/or zinc vacancies V_{Zn} , located mainly on the ZnO surface.

Discussion

Obviously, different conditions of solvothermal syntheses have an influence on the structural and optical

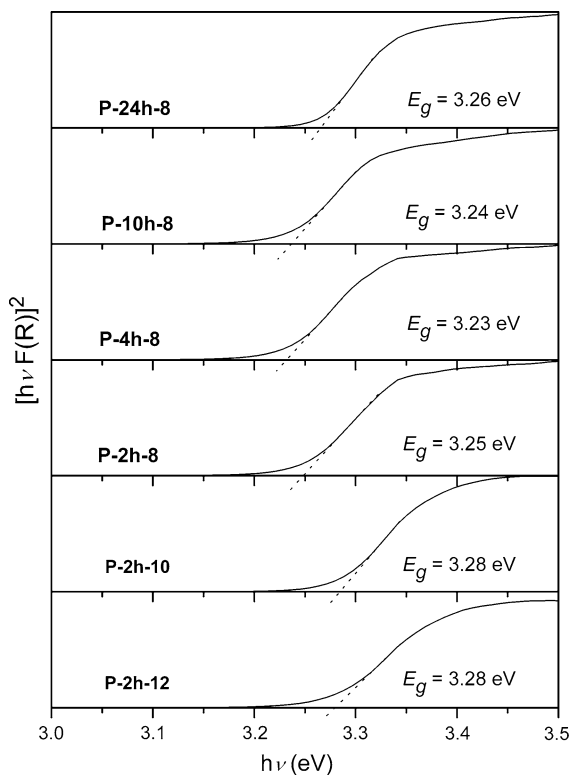


Fig. 5 Tauc plots of ZnO powders synthesized in solvothermal reactions

Table 3 The values of the energy band gap (E_g) and the energy values that correspond to the maxima of the orange (E_{orang}) and green (E_{green}) PL emission peaks for solvothermally synthesized ZnO powders. The differences between E_g and E_{orang} (E_{green}) are also listed

ZnO powders	E_g (eV)	E_{orang} (eV)	E_{green} (eV)	$E_g - E_{\text{orang}}$ (eV)	$E_g - E_{\text{green}}$ (eV)
P-2h-12	3.28	2.02	2.34	1.26	0.94
P-2h-10	3.28	2.02	2.40	1.26	0.88
P-2h-8	3.25	2.05	2.42	1.20	0.83
P-4h-8	3.23	2.04	2.44	1.19	0.79
P-10h-8	3.24	2.07	2.46	1.17	0.78
P-24h-8	3.26	2.03	2.43	1.23	0.83

properties of ZnO powders. The size, shape, and defect structure of solvothermally synthesized ZnO particles were determined largely by corresponding growth mechanism which is highly dependent on temperature, time of the reaction, and pH value of the precursor.

The intensity ratio of the XRD peaks (Fig. 1) for ZnO powders indicates that the degree of crystallinity

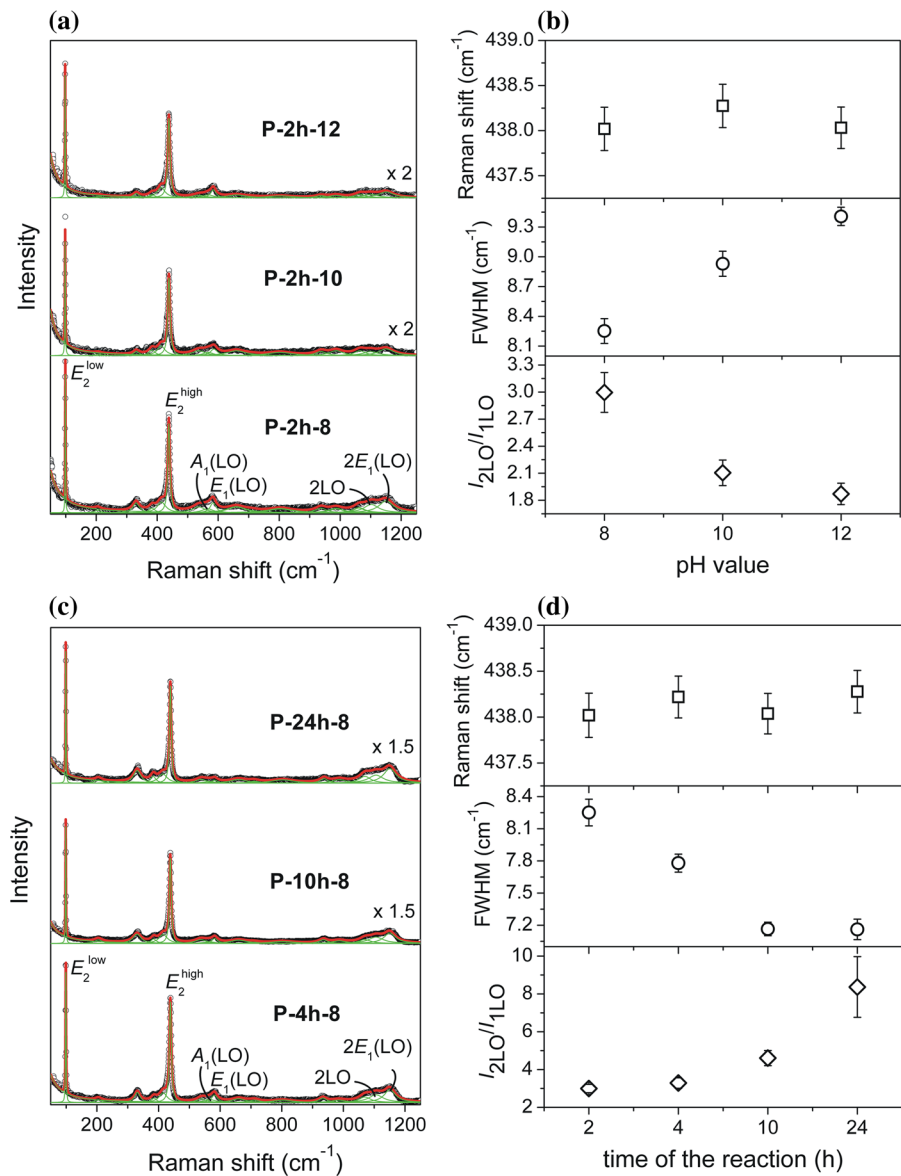
decreases with the increase of pH value from 8 to 10 and 12. The Scherrer analysis shows the average crystallite size, also, decreases when the precursor became highly basic, but it is not less than 19 nm.

The slight differences between values of energy gap of ZnO powders (Table 3), derived from UV-vis DR spectra analysis, most likely originate from defective structure and morphology. There is no apparent trend in the change of energy gap width by varying pH value and time of the reaction. It can be explained by partial compensation of two opposing effects: the band gap narrowing induced by the presence of intrinsic defects and band gap widening due to particle size reduction, knowing that in our ZnO powders, decreasing of the particles' size is accompanied by increasing of defect concentration. Considering that all band gap widths are less than band gap width of bulk (3.37 eV), we believe that the influence of defects in ZnO lattice is dominant for all synthesized ZnO powders.

Increase of the E_2^{high} linewidth and decrease of the Raman modes intensity ratio, $I_{2\text{LO}}/I_{1\text{LO}}$, (Fig. 6b) unambiguously point to increasing of structural disorder and defect concentration with the increase of pH value. On the other side, decrease of the E_2^{high} linewidth and increase of $I_{2\text{LO}}/I_{1\text{LO}}$ intensity ratio (Fig. 6d) indicate improvement of structural ordering and decrease of defect concentration with extension of time of solvothermal reaction. The lack of any significant E_2^{high} frequency shift (Fig. 6b, d) indicates that defects present in the synthesized powders do not cause decrease of correlation length in ZnO crystal lattice. This can be an indication that oxygen vacancies are not dominant type of intrinsic defects in the crystalline structure of synthesized ZnO powders, because great concentration of such defects should be accompanied by E_2^{high} frequency redshift due to decrease of correlation length (Šćepanović et al. 2010).

Knowing that the solvothermal syntheses occur under elevated pressure and temperature in the sealed tank, where all products of the reaction were trapped in the vessel, we can consider that these conditions were suitable for the creation of various types of intrinsic defects in ZnO lattice. The large width of the PL peaks also points to the presence of different intrinsic defects. However, it is expected that the defects inherent to the oxygen-rich conditions dominate in the air atmosphere of the autoclave. Interstitial oxygen, as a shallow acceptor energy level (Wang et al. 2007),

Fig. 6 (Color online) Raman spectra of solvothermally synthesized ZnO powders obtained by varying the pH value (a) and time of the reaction (c). Experimental spectra filled circle are fitted on sum (thick line) of Lorentzian functions (thin line). Dependence of the frequency open square and FWHM open circle of E_2^{high} Raman mode and intensity mode ratio $I_{2\text{LO}}/I_{1\text{LO}}$ open diamond on the pH value (b) and time of the reaction (d) of ZnO powders. The error bars correspond to the standard errors of the parameters in the fitting procedure, superimposed on the experimental error ($\pm 0.2 \text{ cm}^{-1}$) for the E_2^{high} mode frequency

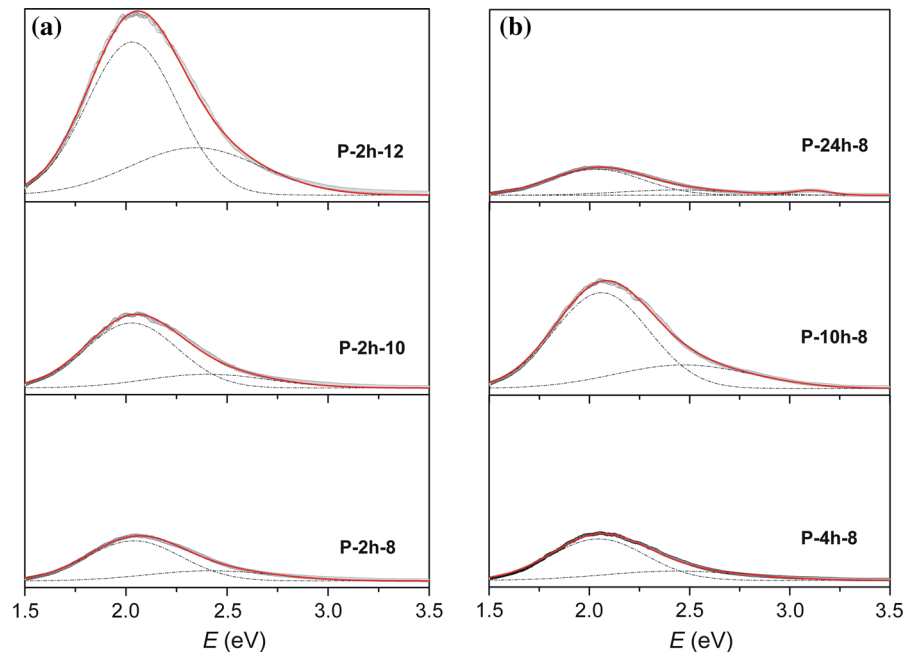


has significant impact on the occurrence of dominant (orange) PL emission, whereas the zinc vacancies, as a deep acceptor energy level (Mhlongo et al. 2014), mostly contribute to the less pronounced (green) emission. Weak UV emission at about 3.10 eV, which can be ascribed to the near-band-edge emission of the wide band gap of the ZnO resulting from the recombination of excitons (Wu et al. 2006), is present only in PL spectrum of powder P-24h-8 and confirms its good crystalline quality.

Inserting of oxygen in the interstitial positions of the crystal lattice generates the displacement of some

atoms from their regular positions. Consequently, slight changes of unit cells' volume can be observed due to the presence of oxygen interstitials. According to the first-principles study of the electronic structure of native point defects in ZnO (Janotti and Van de Walle 2007; Janotti and Van de Walle 2009), it was found that $\text{O}_i\text{-Zn}$ distances are almost equal to d_0 (d_0 is the equilibrium Zn-O bond length along the c -axis). Concurrently, the presence of zinc vacancies results in large increase in the distance Zn-O and equals to 1.1 d_0 . Relatively small values of unit cell volume change (ΔV) for all investigated ZnO powders (Table 2) are in

Fig. 7 (Color online) PL spectra of ZnO powders *open circles*—experimental points, *dash-dot lines*—Gaussian peaks, *red solid lines*—fitting curves for PL spectra



agreement with our assumption that oxygen interstitials are dominant intrinsic defects in solvothermally synthesized ZnO powders.

We have already noticed (Luković Golić et al. 2012) that the growth mechanisms significantly differ depending on the precursor pH value. Crystal-growth process in the cases of pH value equal to 10 and 12 includes rapid nucleation (due to the high concentration of OH^- ions) and particle growth (via complete dissolution process of $\text{Zn}(\text{OH})_2$ due to OH^- ions) which result in small, rounded ZnO particles. A large number of nucleation centers cause more pronounced defective structure for powders P-2h-10 and P-2h-12 than for powders obtained from the slightly basic (pH = 8) precursors. This assumption is also in accordance with the results of Raman and PL spectra analyses which indicate that the powders obtained from highly basic precursors have the lowest crystallinity and the largest deviation from the regular crystal structure.

The growth mechanisms responsible for the formation of powders from the slightly basic precursors (pH = 8) and during the prolonged time of the reactions include the processes of dissolution/recrystallization and oriented attachments. According to the results of TEM and Raman spectra analyzes, we concluded that these processes lead to the formation of well-defined, hexagonal shapes accompanied by the

improvement of crystal lattice ordering when the time of reaction ranges from 2 h to 10 h. The rod-like particles were formed during 24 h owing to the dominant growth rate along {001} direction in wurtzite ZnO crystal. On the other hand, the intensities of PL emissions mainly indicate the improvement of crystalline quality with increase of the reaction time. Only for the sample P-10h-8, we obtained PL emission intensities higher than for the samples with shorter reaction time (P-4h-8 and P-2h-8). Enhanced PL emission for this sample may be related to the coexistence of particles with different shapes and sizes, indicating the coexistence of different growth mechanisms (oriented aggregation, preferential growth along C-axis) (Luković Golić et al. 2012). In our opinion, such a situation was more favorable for the creation of intrinsic defects. Finally, all experimental analyzes of the powder P-24h-8 gave results which indicate the same conclusion—this powder has the most regular crystal lattice with the minimal concentration of the intrinsic defects. This may be related to the dominant growth process—preferential growth along the C-axis which results in large number of rod-like particles and the smallest concentration of defects in crystal lattice. It is obvious that extension of time reaction favors the longitudinal growth along the direction of polar planes of wurtzite crystal. The growth pattern, inherent for ZnO wurtzite lattice,

provides the microstructure with the least free energy of powder system, determined by conditions of the reaction. It can be supposed that a great extension of the reaction time under specified conditions causes the formation of ZnO particles characterized by the highest crystallinity degree and the lowest defect concentration due to preferential growth.

Conclusion

The morphology, particle size, and defective structure of solvothermally synthesized ZnO powders could be modified by varying the temperature, time of the reaction, and pH value of the precursor. Different conditions of reactions influence the processes taking place during particles growth. Structural characterizations (XRD, Raman spectroscopy, and PL spectroscopy) confirmed that concentration of defects slightly enlarges as pH value of the precursor increases from 8 to 12. Prolongation of the reaction time in slightly basic precursors results in the improvement of the crystallinity. The ZnO powder with the most ordered structure and the least concentration of defects was synthesized during 24 h at 200 °C. Raman and PL spectra analyses suggest that oxygen interstitials most likely represent the dominant type of defects in wurtzite lattice of solvothermally synthesized ZnO powders.

We have shown that conditions of solvothermal syntheses determine the structural, morphological, and optical properties of ZnO powders, arising as a result of the inherent growth mechanisms. Presented results indicate that these properties of ZnO particles are mostly dependent on pH value of the precursor due to substantial differences in the type of growth processes.

Acknowledgments The authors acknowledge the financial support of the Ministry of Education and Science of Republic of Serbia (project number III45007).

References

- Cai JW, Xu JP, Zhang XS, Niu XP, Xing TY, Ji T, Li L (2012) Defect-related visible luminescence of ZnO nanorods annealed in oxygen ambient. *Optoelectronics Lett* 8:4–8
- Cusco R, Alarcon-Llado E, Ibanez J, Artus L, Jimenez J, Wang B, Callahan MJ (2007) Temperature dependence of Raman scattering in ZnO. *Phys Rev B* 75:165202
- Djurišić A, Leung YH (2006) Optical properties of ZnO nanostructures. *Small* 2:944–961
- Djurišić AB, Leung YH, Tam KH, Ding L, Gem WK, Chen HY, Gwo S (2006) Green, yellow and orange defect emission from ZnO nanostructures: influence of excitation wavelength. *Appl Phys Lett* 88:103107
- Dutta S, Chattopadhyay S, Sarkar A, Chakrabarti M, Sanyal D, Jana D (2009) Role of defects in tailoring structural, electrical and optical properties of ZnO. *Prog Mater Sci* 54:89–136
- Garvey RG (1986) LSUCRIPC least-squares unit-cell refinement with indexing on the personal computer. *Powder Diffraction* 1:114–116
- Ghosh S, Khan GG, Varma S, Mandal K (2013) Influence of film thickness and oxygen partial pressure on cation-defect induced intrinsic ferromagnetic behavior in luminescent P-type Na-Doped ZnO thin films. *ACS Appl Mater Interfaces* 5:2455–2461
- Greene LE, Law M, Goldberger J, Kim F, Johnson JC, Zhang Y, Saykally RJ, Yang P (2003) Low-Temperature wafer-scale production of ZnO nanowire arrays. *Angew Chem Int Ed* 42:3031–3034
- Jagadish C, Pearson SJ (2006) Zinc Oxide bulk, thin films and nanostructures. Elsevier, New York
- Janotti A, Van de Walle CG (2007) Native point defects in ZnO. *Phys Rev B* 76:165202
- Janotti A, Van de Walle CG (2009) Fundamentals of zinc oxide as a semiconductor. *Rep Prog Phys* 72:126501
- Kumar SS, Venkateswarlu P, Rao VR, Rao GN (2013) Synthesis, characterization and optical properties of ZnO nanoparticles. *Int Nano Lett* 3:30
- Lin KF, Cheng HM, Hsu HC, Lin JL, Hsieh WF (2005) Band gap variation of size-controlled ZnO quantum dots synthesized by sol-gel method. *Chem Phys Lett* 409:208–211
- Luković Golić D, Branković G, Počuča-Nešić M, Vojisavljević K, Rečnik A, Daneu N, Bernik S, Šćepanović M, Poleti D, Branković Z (2011) Structural characterization of self-assembled ZnO nanoparticles obtained by the sol-gel method from $\text{Zn}(\text{CH}_3\text{COO})_2 \cdot 2\text{H}_2\text{O}$. *Nanotechnology* 22:395603
- Luković Golić D, Branković Z, Daneu N, Bernik S, Branković G (2012) Solvothermal syntheses of nano- and micro-sized ZnO powders with a controllable morphology. *J Sol-Gel Sci Technol* 63:116–125
- Mang A, Reimann K, Rübenacke St (1995) Band gaps, crystal-field splitting, spin-orbit coupling, and exciton binding energies in ZnO under hydrostatic pressure. *Solid State Commun* 94:251–254
- Mhlongo GH, Motaung DE, Nkosi SS, Swart HC, Malgas GF, Hillie KT, Mwakikunga BW (2014) Temperature-dependence on the structural, optical and paramagnetic properties of ZnO nanostructures. *Appl Surf Sci* 293:62–70
- Motaung DE, Mhlongo GH, Nkosi SS, Malgas GF, Mwakikunga B, Coetsee E, Swart HC, Abdallah HMI, Moyo T, Ray SS (2014) Shape-selective dependence of room temperature ferromagnetism induced by hierarchical ZnO nanostructures. *ACS Appl Mater Interfaces* 6:8981–8995
- Nickel NH, Terukov E (2005) Zinc Oxide—A material for micro- and optoelectronic applications. Springer, Netherlands
- Panigrahy B, Aslam M, Misra DS, Ghosh M, Bahadur D (2010) Defect-Related emission and magnetization properties of ZnO nanorods. *Adv Funct Mater* 20:1161–1165

- Roth AP, Webb JB, Williams DF (1982) Band-gap narrowing in heavily defect doped ZnO. *Phys Rev B* 25:7836–7839
- Šćepanović M, Grujić Brojčin M, Vojisavljević K, Bernik S, Srećković T (2010) Raman study of structural disorder in ZnO nanopowders. *J Raman Spectrosc* 41:914–921
- Šćepanović M, Grujić Brojčin M, Vojisavljević K, Srećković T (2011) Defect induced variation in vibrational and optoelectronic properties of nanocrystalline ZnO powders. *J Appl Phys* 109:034313
- Shim ES, Kang HS, Pang SS, Kang JS, Yun I, Lee SY (2003) Annealing effect on the structural and optical properties of ZnO thin film on InP. *Mater Sci Eng B-Adv* 102:366–369
- Sim AYL, Goh GKL, Tripathy S, Andeen D, Lange FF (2007) Photoluminescence of hydrothermally epitaxied ZnO films. *Electrochim Acta* 52:2933–2937
- Spanhel L, Anderson M (1991) Semiconductor clusters in the sol-gel process: quantized aggregation, gelation, and crystal growth in concentrated ZnO colloids. *J Am Chem Soc* 113:2826–2833
- Studenikin SA, Golego N, Cocivera M (1998) Fabrication of green and orange photoluminescent, undoped ZnO films using spray pyrolysis. *J Appl Phys* 84:2287
- Wang HQ, Wang GZ, Jia LC, Tang CJ, Li GH (2007) Polychromatic visible photoluminescence in porous ZnO nanotubes. *J Phys D Appl Phys* 40:6549–6553
- Wood DL, Tauc J (1972) Weak absorption tails in amorphous semiconductors. *Phys Rev B* 5:3144–3151
- Wu L, Wu Y, Pan X, Kong F (2006) Synthesis of ZnO nanorod and the annealing effect on its photoluminescence property. *Opt Mater* 28:418–422